

Chapter 17

MRI Phenotyping of Genetically Altered Mice

Jason P. Lerch, John G. Sled, and R. Mark Henkelman

Abstract

The laboratory mouse, with its genetic similarity to humans and rich set of tools for manipulating its genome, has emerged as one of the key models for experimental investigation of the genotype/phenotype relationships in mammals. Recent innovations have made MRI an increasingly popular tool for examining the phenotype of genetically altered mice. Advances in field strengths, mouse handling, image analysis and statistics have contributed greatly in this regard. In this chapter, we illustrate the methods necessary to achieve high-throughput phenotyping of genetically altered mice using multiple-mouse MRI combined with advanced image analysis techniques and statistics.

Key words: Magnetic resonance imaging, phenotyping, mouse models, genetics.

1. Introduction

The completion of the human genome sequence in the century just past presents a major challenge for biomedical research in the twenty-first century: that of understanding the relationship of detailed genetic sequences both to the normal development of the human individual and to the propensity for disease development. From a biomedical perspective, this genotype/phenotype relationship needs to be understood for the human species. However, the limited ability to do genetic experiments in the human means that much of this relationship will be worked out instead in the mouse. Mice have very similar genetics to that of the human with a 99.5% ability to recognize equivalent genes from one species to the other (1). Mice show many of the symptoms of both the rare and common human diseases. Existing inbred strains of mice provide homogeneous genetic backgrounds making genetic

modifications readily identifiable. There exist remarkably sophisticated genetic tools for manipulating genetics in the mouse. Finally, the rapid reproduction time and the comparatively low housing costs make the mouse an ideal model for experimental investigation of the genotype/phenotype relationships in the mammal.

Magnetic resonance imaging (MRI) is an excellent modality for investigating genetically altered animals. It is capable of whole brain coverage, can be used *in vivo* and provides multiple contrast mechanisms for investigating different aspects of neuroanatomy and physiology. The advent of high-field scanners along with the ability to scan multiple mice simultaneously (2–4) allows for rapid phenotyping of novel mutations in ways heretofore not possible.

2. Materials

2.1. Mice

Groups of genetically or environmentally modified mice are otherwise identical to control animals not having the modification. Typically, inbred background strains are chosen due to their highly conserved neuroanatomy (5).

2.2. MRI Hardware

1. An MR imager of 7 T or higher field strength with as high a performance gradient system as can be obtained.
2. An array of closely coupled radiofrequency coils and an array of spectrometers for multiple mouse imaging (e.g. Varian Direct Drive) (4). The coils need to be isolated from each other and operate in both transmit and receive. Spatial uniformity of coils is important for automated computer image processing (*see Note 1*).
3. Mouse holders incorporating physiological monitoring (cardiac, respiration, temperature, blood oxygenation, etc.), as well as gaseous anaesthetic and oxygen (6).

2.3. Computer Hardware

1. A cluster of Linux workstations containing at least 2 GB of memory per processor (*see Note 2*).
2. Networked disk storage with at least 3 GB of storage capacity per brain to be analysed.
3. Visualization workstations to analyse the data (*see Note 3*).

2.4. Software

1. A modern Linux distribution with a full set of C/C++ compilers and scripting languages (Bash, Perl, Python).
2. Sun Grid Engine (<http://gridengine.sunsource.net>) for distributing work across the Linux cluster.

3. The MINC toolkit (<http://www.bic.mni.mcgill.ca/software>) and ANIMAL registration software (7, 8) (see Note 4).

3. Methods

Mouse phenotyping using MRI can be divided into four sub-parts (1): mouse preparation (2), MR acquisition (see Figs. 17.1 and 17.2) (3), image processing (see Fig. 17.3) and (4) statistical analysis. The goal is to acquire the best data possible within the available time, to accurately define the anatomical correspondence between the different images and to identify any statistically significant differences between the groups of mice. Differences may exist in MRI signal intensities, derived measures such as fractional anisotropy or metrics of brain shape.

Image registration, the task of finding anatomical correspondence between the image, can be divided into three stages: an initial rigid body alignment of all images to a pre-existing target

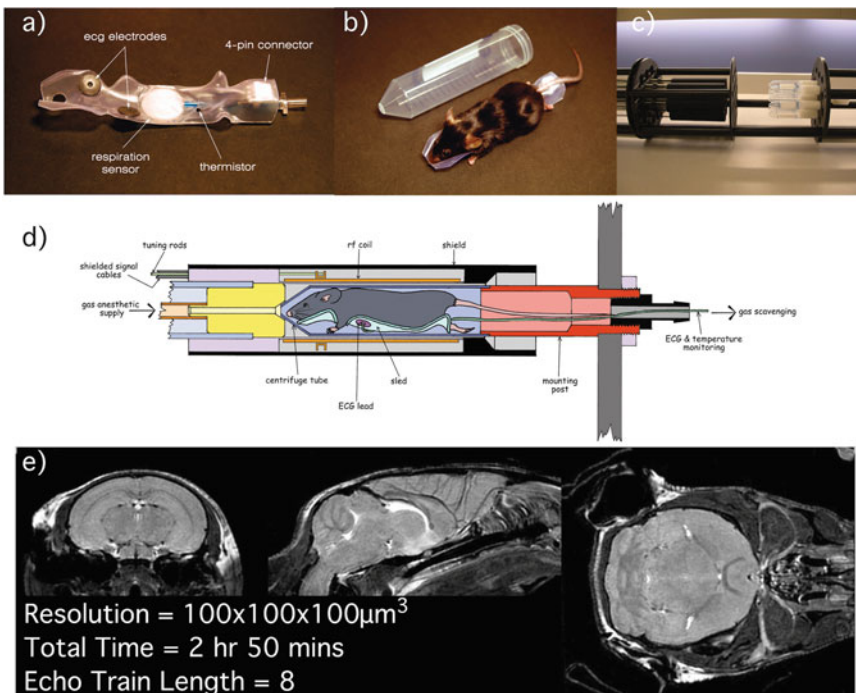


Fig. 17.1. The in vivo MR imaging setup consists of a custom-moulded sled (a), upon which the mouse is placed and enclosed within a test tube (b). Up to 16 mice can be scanned at once (c). Once inside the scanner, gas anaesthesia is continuously administered and key bodily functions monitored (d). Three slices through an example image are shown in (e).

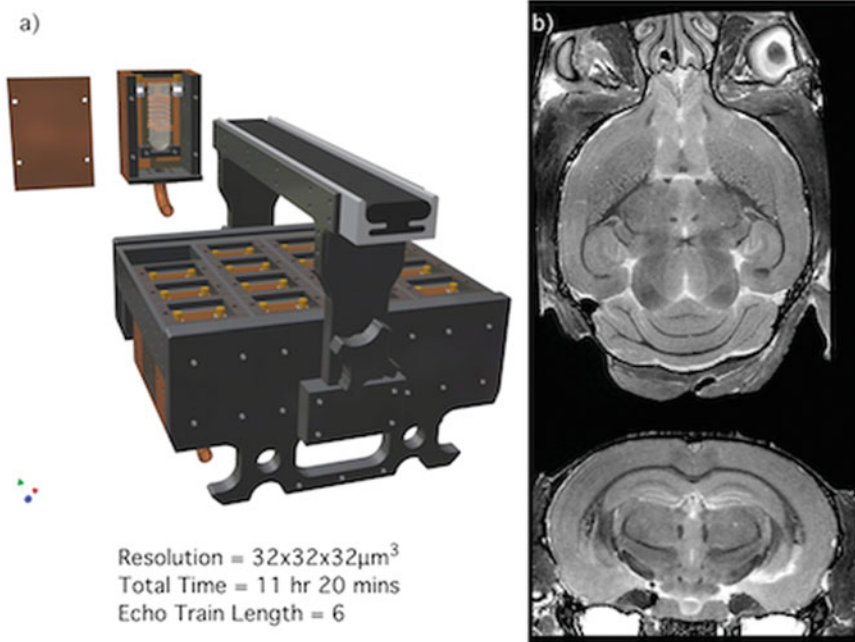


Fig. 17.2. The ex vivo consists of 16 independent solenoid coils assembled into an array (a). Two example slices of an overnight acquisition of a fixed brain are shown in (b).

establishing the pose and coordinate system of the analysis, pairwise 12-parameter registration to create a groupwise atlas of all images in the dataset being analysed and a series of iterative non-linear registrations resulting in a model-independent atlas of that dataset. The points below will address these steps in greater detail; it is important to note, however, that in practice they are all incorporated into a single pipeline environment and each step is not separately executed by the user (*see Note 5*).

3.1. Mouse Preparation

1. *Live mice.* Live mice are anaesthetized with 3% isoflourane in warm air, injected with 0.5 ml of saline to maintain hydration, shaved along the chest to provide contact with the ECG electrodes, placed on a moulded sled to provide uniform posture, restrained with a Velcro strap over the head and inserted into 50 ml centrifuge tubes with a hole drilled in the end to provide anaesthetic. After insertion into the RF coils in the magnet, 1% isoflourane mixed with oxygen is provided to maintain the anaesthesia. Warmed air is blown into the magnet to maintain an ambient temperature of 27 °C.
2. *Fixed Brains.* To provide better resolution and SNR and to avoid motion artefacts, mouse brains are fixed and scanned overnight. Mice are anaesthetized with a combination of Ketamine (Pfizer, Kirkland, QC) (100 mg/kg) and Rompun

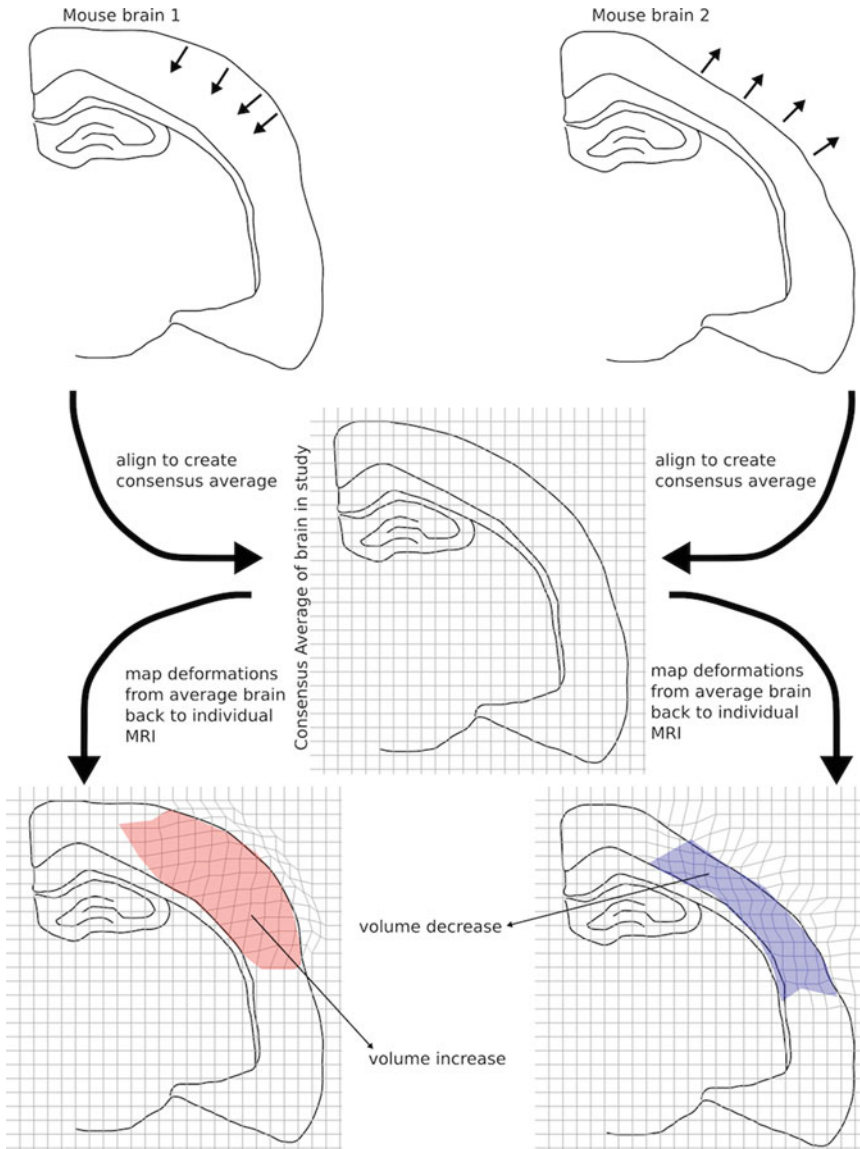


Fig. 17.3. This figure illustrates the derivation of local volume changes used throughout the study. Two *line drawings* of the brain are shown on *top*, one with an increased cortical volume and the other with decreased cortical volume. These images are then aligned to create a consensus average, shown in the *middle* with the deformation grid superimposed. The deformations are then inverted to map back to the individual brains; the distortions in the grid can be seen in the *bottom* of the figure, with *shaded areas* indicating local volume increase and decrease inside the brain.

(Bayer Inc., Toronto, ON) (20 mg/kg) via intraperitoneal injection. Thoracic cavities are opened and animals are perfused through the left cardiac ventricle with 30 mL of phosphate-buffered saline (PBS) (pH 7.4) at room temperature (25 °C) at a rate of approximately 100 mL/h (*see Note 6*). This is followed by infusion with 30 mL of iced

4% paraformaldehyde (PFA) plus 2 mM ProHance in PBS at the same rate. Following perfusion, the heads are removed along with the skin, lower jaw, ears, and the cartilaginous nose tip. The remaining skull structures are allowed to postfix in 4% PFA plus 2 mM ProHance at 4 °C for 12 h. The skulls are then transferred to solution containing 1X PBS + 0.02% sodium azide + 2 mM ProHance for 4 days at 15°C. MRIs can then be acquired no sooner than 4 days and not longer than 2.5 months postfixation.

3.2. MR Acquisition

1. MR images are acquired using pulse sequences that provide appropriate contrast for the phenotype that is being investigated. For anatomical images and analyses, fast spin echo (turbo spin echo) or gradient echo scans are efficient and typically used. Isotropic voxels from 3D acquisitions are preferable to multi-slice imaging when computer analysis is being used. Whatever the acquisition, excess SNR should be spent on improved resolution until the SNR is approximately 20, the value which provides an optimal tradeoff for computer registration (9). Representative examples of scan quality can be seen in Figs. 17.1 and 17.2, respectively, for in vivo and ex vivo protocols (*see Note 7*).
2. Calibration and compensation for geometric distortion may be required to obtain geometric accuracy comparable to the morphological differences of interest. The presence of geometric distortions is readily assessed by scanning an object of known geometry immersed in solution. Postprocessing for geometric distortion is typically available from the MRI scanner vendor or can be implemented by identifying known landmarks on a test object (*see Note 8*).

3.3. Image Processing

1. Six-parameter registration: the goal is to rigidly align all scans in a study into the same coordinate space.
 - 1.1. Create a series of Gaussian blurred representations of the input data and the atlas (*see Note 9*).
 - 1.2. Align each blurred representation to the equivalently blurred version of the atlas using six degrees of freedom (three rotations, three scales; referred to as lsq6 from hereon). The first blur can be initialized with either a centre-of-gravity estimation or an identity transform (*see Note 9*); each subsequent registration is initialized with the previous registration transform.
 - 1.3. Resample the data with the final transform from step 1.2.
 - 1.4. Remove any intensity inhomogeneities using the N3 algorithm (10).

2. At this point, all the scans are in the same space and orientation. The next step is to create the best possible linear model of all the brains contained in this dataset.
 - 2.1. Create a series of Gaussian blurred representations of the lsq6-resampled datasets using FWHM 0.3, 0.2 and 0.15 mm kernels. Take the gradient of the blur for the FWHM 0.2 mm dataset.
 - 2.2. Align each scan towards every other scan in the dataset. That is, assuming five scans in the study, scan 1 will be separately aligned to scans 2, 3, 4 and 5. For each pair, three separate registrations are computed, starting with the FWHM 0.3 mm kernel initialized by an identity transform, followed by the gradient of the FWHM 0.2 mm kernel initialized by the previous registration and finalized by the FWHM 0.15 mm kernel. Each registration has 12 degrees of freedom (three rotations, three translation, three scales and three shears, referred to as lsq12 from hereon). The average transform for all pairs is then computed, i.e. staying with the above cited example, scan 1 was separately aligned towards scans 2, 3, 4 and 5; the four resulting transforms are then averaged (*see Note 10*).
 - 2.3. Resample each scan with the transform resulting from step 2.2.
 - 2.4. Average all of the resampled images from step 2.3 to create a study-population-specific atlas (lsq12 atlas).
3. The third step is to refine the registration by locally deforming the scans to bring them into exact correspondence. This is done using an iterative process, each time aligning the scans towards the model created by the previous iteration.
 - 3.1. Create a series of blurred representations of the individual lsq12 resampled images, as well as the lsq12 atlas.
 - 3.2. Deform each lsq12 resampled image towards the lsq12 atlas.
 - 3.3. Resample each image with the transform from step 3.2.
 - 3.4. Average all of the resampled images from step 3.3 to create the first non-linear version of the study-population-specific atlas.
 - 3.5. Repeat steps 3.1 through 3.4, this time substituting the first non-linear resampled images and atlas for the lsq12 images and atlas. This process is repeated six times with the registration parameters taken from **Table 17.1**.

Table 17.1
Parameters used for non-linear registration

Generation	Blurring kernel (mm)	Step size (mm)	Registration target	Iterations
1	0.3	0.7	LSQ12	20
2	0.2	0.6	Generation 1	6
3	0.2	0.5	Generation 2	8
4	0.2	0.24	Generation 3	8
5	0.1	0.12	Generation 4	8
6	0.06	0.06	Generation 5	8

4. The fourth step is to prepare data for statistical analysis. The end result of this step is a series of parametric maps that define the shape of the brain as accurately and comprehensively as possible.
 - 4.1. Find any remaining linear components of the final non-linear transform that maps the lsq12 aligned images to the non-linear average. This is accomplished by selecting 20,000 randomly placed points in the brain and extracting their spatial coordinates before and after non-linear resampling. The best possible 12-parameter fit is then estimated from this point set and subtracted from the final non-linear transform, resulting in a displacement field containing the pure non-linear component of the registration.
 - 4.2. These pure non-linear displacement fields are then centred with respect to the population mean by computing the mean displacement vector at each voxel and subtracting it from every scan's displacement field.
 - 4.3. The centred displacement fields are then smoothed using a series of Gaussian blurring kernels (*see Note 11*).
 - 4.4. Next, derive two metrics from each of the smoothed displacement fields: the Jacobian determinant (**11**) a measure of local volume expansion and contraction, as well as the magnitude of the deformation at each voxel (*see Note 12*).
 - 4.5. Multiply the Jacobian determinants with the scale factor determined from the 12 parameter registration. This results in two parametric maps per smoothed displacement field: the normalized Jacobian determinant, which describes local volume differences after

overall brain size has been normalized, and the absolute Jacobian determinant, which incorporates both the local volume change and brain size differences at every voxel.

- 4.6. Align a segmented atlas dividing the brain into 62 separate structures (114 if bilateral structures are separated into left and right) onto the final non-linear study-population-specific atlas (12).
- 4.7. Using the smallest smoothed displacement vector, integrate the Jacobian determinant multiplied by the voxel size across each structure to give a structure volume in cubic millimetre.
- 4.8. Use the transform taking each scan from native (scanner) space to the non-linear average to resample any associated data with the scan, i.e. this might include blood flow maps derived from Arterial Spin Labelling, fractional anisotropy or related measures from Diffusion Tensor Imaging, etc.

3.4. Statistical Analysis

The registration pipeline described above results in (1) a table of anatomical structure volumes (2), measures of local expansion and contraction at every voxel (3), deformation vectors at every voxel, and (4) associated data resampled into the space of the non-linear average. The next set of steps determines whether there are any statistically significant differences in these measures between genotypes or other natural groupings of the animals (environment, gender, etc.).

1. Create a spreadsheet containing information about each scan (genotype, bodyweight, age of the animal, etc.).
2. Load the spreadsheet in software capable of performing statistical analyses across imaging volumes – we use RMINC for this purpose (*see Note 13*).
3. All subsequent tests are performed using variants of linear models (*see Note 14*).
 - 3.1. Comparisons of differences in overall brain volume and volumes of individual brain structures.
 - 3.2. Analyses of the same model at every voxel using the log-transformed Jacobian determinants of the blurred displacement fields.
 - 3.3. Analyses of co-registered data (perfusion maps, FA maps, etc.)
4. Comparisons of the deformation vectors themselves are carried out using Hotelling's T^2 statistic – though this is only applicable for the simple two-group comparison.

5. Once all statistical tests are done, collect all of the resulting p-values and threshold them using the False Discovery Rate (FDR) (13) in order to control the number of false positives due to multiple comparisons (*see* **Note 15**).
6. Imaging data are typically analysed in an exploratory manner through a continuous process of refining statistical models. After the first five steps, the key is to now investigate individual regions that were found significant or, as importantly, were hypothesized to be significant, but did not survive multiple comparisons, and to examine the distributions of the data at specific voxels. In particular, one should check for
 - 6.1. Outliers: outliers can significantly affect data analyses. We have found two main reasons for outliers in our data: (1) misregistration, which happens rarely, but still needs to be checked; and (2) biological; at times a whole litter of mice will have considerably smaller brains for no discernible reasons.
 - 6.2. Necessary covariates: confounding factors can easily spoil an analysis; for example, one of the most difficult confounds we encounter is that of body-weight/brain volume covariation. If the brains in a particular mutation are smaller, one needs to rule out that the whole mouse is not smaller with the implication that there is nothing unique about the findings in the brain. Other important checks are for gender balance, consistent ages, etc.

4. Notes

1. Considerable SNR advantages can be gained by construction of application-specific close-fitting solenoid coils for specimen scanning. An array of custom-built 14-mm diameter solenoid coils with a length of 18.3 mm and over wound ends provides for convenient scanning of multiple brain-in-skull specimens (*see* **Fig. 17.2**).
2. The software that we use runs just as happily on OS X and can be made to work on Windows as well. In our experience, however, a Linux cluster is the easiest to maintain for these types of computational problems.
3. If using Linux, we highly recommend using NVidia graphics cards with the NVidia OpenGL drivers; for all the system administration headaches that these proprietary drivers

- can cause, they still do provide the best performance for 3D rendering on Linux.
4. The recipe given herein for phenotyping genetically altered mice is quite obviously based on our work. Needless to say, the overall approach that we are using is clearly compatible with other software toolkits.
 5. Our pipeline environment, named MICe-build-model (<https://wiki.phenogenomics.ca/display/MICePub/MICe-build-model>), is freely available to the research community; interested users should contact the authors of this chapter in order to obtain the software.
 6. Leakage of CSF from fixed brains must be carefully avoided, since it leads to air bubbles in the sample with associated susceptibility artefacts. Inadvertent bubbles can be removed by immersing samples in phosphate-buffered saline with the brainstem vertical and applying multiple cycles of vacuum pumping.
 7. Scan parameters for the images shown in **Fig. 17.1** were a T2-weighted, 3D fast spin echo sequence with eight echoes, TR/TE = 900/12 ms, two averages, field-of-view $24 \times 24 \times 40 \text{ mm}^3$ and matrix size = $240 \times 240 \times 400$ giving an image with $100 \mu\text{m}$ isotropic voxel and a total scan time of 2.8 h; and those shown in **Fig. 17.2** were a T2-weighted, 3D fast spin echo sequence with six echoes, TR/TE = 325/32 ms, four averages, field-of-view $14 \times 14 \times 25 \text{ mm}^3$ and matrix size = $432 \times 432 \times 780$ giving an image with $32 \mu\text{m}$ isotropic voxel and total imaging time of 11.3 h. Long scans such as the latter should be implemented to be insensitive to drift in the magnet and DC offsets in the RF receivers.
 8. Tensor cubic b-spline approximation is a robust means of estimating a non-linear distortion field based on landmarks. An implementation can be found at <https://wiki.phenogenomics.ca>.
 9. The blurring kernel varies by the type of input data; in the common case of scans originating from the same scanner with care taken to ensure that the head is in a similar position then two blurs of FWHM 0.5 mm and 0.3 mm are sufficient. If the data are more disparate, which can occur with fixed sample scans and/or if the data originate from different scanners, then an initial centre-of-gravity estimation followed by a larger set of kernels (FWHM 5, 1, 0.5, 0.3 mm) is needed.
 10. We found that using these pairwise registration results in a considerably improved representation of the data than

to continue aligning each scan towards the atlas. We are indebted to Andrew Janke and Paul Thompson for the matrix averaging code/mathematics.

11. As with most brain imaging analysis, the choice of blurring kernels is a bit of a black art. We tend to blur with 0.1, 0.2, 0.5 and 1.0 mm kernels and rely on the 0.5 mm for the bulk of our analyses. The larger kernel is useful for looking at very diffuse changes and the smaller ones for very focal differences.
12. We define displacement and Jacobian determinant such that the identity transformation corresponds to 0 displacement and a Jacobian determinant of 1.
13. Find out more about RMINC at <http://launchpad.net/rminc>. Many other software packages are capable of carrying out the same analyses.
14. The main variation on the linear model employed is the mixed-effects linear model, which correctly models inter-relationships in the data that occur by, for example, having multiple time points for some of the animals in the study.
15. We tend to use both FDR and, on occasion, more stringent Family Wise Error Rate (FWER) correction techniques (14) such as permutation testing (15) and Random Field Theory (16). In our experience with phenotyping, especially when dealing with novel mutations, the role of MRI is primarily to generate hypotheses which will often be followed up using other techniques, including immunohistochemistry, electrophysiology. The more lenient FDR is therefore well suited for this task, whereas FWER's more stringent threshold risks leave too many false negatives.

Acknowledgments

Many of the present and previous members of the Mouse Imaging Centre (MICe) in Toronto have contributed to the development of these techniques. Many developmental biologists and mouse geneticists from around the world have provided mutant mice for imaging and improved the analysis methods. Funding from the Canadian Foundation for Innovation, the Ontario Research and Development Challenge Fund, the US National Institutes of Health and the Canadian Institutes of Health Research is gratefully acknowledged.

References

1. Waterston, R. H., Lindblad-Toh, K., Birney, E. et al. Initial sequencing and comparative analysis of the mouse genome. *Nature* 2002;420:520–562.
2. Henkelman, R., Dazai, J., Lifschitz, N. et al. High throughput microimaging of the mouse brain. *Proc Int Soc Magn Reson Med* 2006.
3. Nieman, B., Bishop, J., Dazai, J. et al. MR technology for biological studies in mice. *NMR Biomed* 2007;20:291–303.
4. Bock, N., Nieman, B., Bishop, J., Mark Henkelman, R. In vivo multiple-mouse MRI at 7 tesla. *Magn Reson Med* 2005;54:1311–1316.
5. Spring, S., Lerch, J., Henkelman, R. Sexual dimorphism revealed in the structure of the mouse brain using three-dimensional magnetic resonance imaging. *Neuroimage* 2007;35:1424–1433.
6. Dazai, J., Bock, N. A., Nieman, B. J., Davidson, L. M., Henkelman, R. M., Chen, X. J. Multiple mouse biological loading and monitoring system for MRI. *Magn Reson Med* 2004;52:709–715.
7. Collins, D. L., Neelin, P., Peters, T. M., Evans, A. C. Automatic 3d intersubject registration of MR volumetric data in standardized talairach space. *J Comput Assist Tomogr* 1994;18:192–205.
8. Collins, D., Holmes, C., Peters, T. M., Evans, A. Automatic 3-D model-based neuroanatomical segmentation. *Hum Brain Mapp* 1995;3:190–208.
9. Kale, S. C., Lerch, J., Henkelman, R. M., Chen, X. J. Optimization of the SNR-resolution tradeoff for registration of magnetic resonance images. *Hum Brain Mapp* 2008;29:1147–1158.
10. Sled, J. G., Zijdenbos, A. P., Evans, A. C. A nonparametric method for automatic correction of intensity nonuniformity in MRI data. *IEEE Trans Med Imaging* 1998;17:87–97.
11. Chung, M. K., Worsley, K. J., Paus, T. et al. A unified statistical approach to deformation-based morphometry. *Neuroimage* 2001;14:595–606.
12. Dorr, A., Lerch, J., Spring, S., Kabani, N., Henkelman, R. High resolution three-dimensional brain atlas using an average magnetic resonance image of 40 adult C57Bl/6j mice. *Neuroimage* 2008;42:60–69.
13. Genovese, C. R., Lazar, N. A., Nichols, T. Thresholding of statistical maps in functional neuroimaging using the false discovery rate. *Neuroimage* 2002;15:870–878.
14. Nichols, T., Hayasaka, S. Controlling the familywise error rate in functional neuroimaging: A comparative review. *Stat Methods Med Res* 2003;12:419–446.
15. Nichols, T. E., Holmes, A. P. Nonparametric permutation tests for functional neuroimaging: A primer with examples. *Hum Brain Mapp* 2002;15:1–25.
16. Worsley, K. J., Taylor, J. E., Tomaiuolo, F., Lerch, J. Unified univariate and multivariate random field theory. *Neuroimage* 2004;23(Suppl 1):S189–S195.